# $(Ba, Sr)_3MgSi_2O_8$ structure change caused by Ba/Sr replacement

Yoshinori Yonezaki[a)]
*Interdisciplinary Graduate School of Medicine and Engineering, University of Yamanashi, Miyamae 7–32, Kofu 400–8511, Japan*

(Received 22 April 2014; accepted 31 August 2014)

Crystal structure of $Ba_xSr_{3-x}MgSi_2O_8$ has been determined by Raman spectroscopy and X-ray diffraction. The solid solution series have glaserite-type layered structures made of corner-sharing $SiO_4$ tetrahedra and $MgO_6$ octahedra. $Ba^{2+}$ and $Sr^{2+}$ ions are sandwiched in between the layers. Raman spectroscopy has found that structural symmetry changes at $x = 0.5$ and 2.5. Structural refinement by the Rietveld method has clarified that the symmetry changes occur among $C2$ ($Z = 4$), $P\bar{3}m1$ ($Z = 1$), and $P\bar{3}$ ($Z = 3$). They originate in $SiO_4$ tilting caused by size mismatch between alkali–earth cations and their site spaces. For $x \leq 0.5$, $SiO_4$ tilting occur every other interlayer space, whereas for $x \geq 2.5$, all the $SiO_4$ tilt. © *2014 International Centre for Diffraction Data.*
[doi:10.1017/S0885715614000803]

Key words: silicate, crystal structure, Raman spectroscopy, X-ray diffraction

## I. INTRODUCTION

Over the past few decades, bracelet-type $XY[TO_4]$ compounds ($X$, $Y$: 10- and 12-coordinated cations; $T$: tetrahedrally coordinated cation) have attracted scientific attention in the field of structure–property relationships. In particular, glaserite-type oxides, such as $K_3Na(SeO_4)_2$, $K_3Na(CrO_4)_2$, and $K_3Na(MoO_4)_2$, have been intensively studied because their ferroelastic character closely relates to the structural symmetry (Mróz *et al.*, 1992; Krajewski *et al.*, 1993; Kaczmarski *et al.*, 1994; Kaczmarski and Mróz, 1998). Since $K_2SO_4$ was found to be a potential candidate for radiation dosimetry (Gromov and Morton, 1966; Hayakawa and Ohta, 1999; Ohta *et al.*, 2000), this type of compounds has been focused on as optical materials. In recent years, $M_3MgSi_2O_8$ ($M$ = Ba, Sr, Ca) have been studied as host materials for $Eu^{2+}$-activated phosphors (Barry, 1968; Lin *et al.*, 2003; Kim *et al.*, 2005; Jung and Seo, 2006; Okamoto *et al.*, 2008; Yonesaki *et al.*, 2008, 2009; Im *et al.*, 2009; Fu *et al.*, 2010). Their luminescence originates in 5d–4f electron transitions in $Eu^{2+}$ ions. Since energy levels of $Eu^{2+}$ are strongly affected by the crystal-field strength and site symmetry, precise structure analyses are required for $M_3MgSi_2O_8$ to understand the spectroscopic character of $Eu^{2+}$ dopants. In our previous report, the crystal structure was approximately determined for $BaCa_2MgSi_2O_8$ and their derivatives by X-ray powder diffraction technique, and the luminescence properties of $Eu^{2+}$ were discussed in terms of the determined structure (Yonesaki *et al.*, 2008, 2009). $M_3MgSi_2O_8$ has a layered structure (Figure 1). Corner-sharing $SiO_4$ tetrahedra and $MgO_6$ octahedra are polymerized to form the layer. Between the layers, there are three sites for alkali–earth cations; one is at the center of the interlayer space (A-site) and the remaining two are embedded in the layer pockets (B′- and B″-sites). $M_3MgSi_2O_8$ changes its space group, depending on the average size of A-site cations. At the same time, it has been reported that B-site cations also cause layer deformation associated with $SiO_4$ twisting around threefold rotation axis (Park *et al.*, 2011; Yonesaki, 2013). However, such layer deformation could not be identified only with X-ray diffraction (XRD) because of the small X-ray atomic scattering factor of oxygen. Actually Park *et al.* (2011) used neutron powder diffraction to identify the $SiO_4$ twisting in $BaCa_2MgSi_2O_8$. In the present study, Raman spectroscopy and XRD were applied to $Ba_xSr_{3-x}MgSi_2O_8$ solid solution series to elucidate the structure change caused by Ba/Sr-replacement. Vibrational frequencies are very sensitive to interatomic forces and site symmetry. Raman spectroscopy could thus trace small changes in crystal structure, which had been missed in X-ray powder diffraction. Firstly, Raman spectroscopy was applied to $Ba_xSr_{3-x}MgSi_2O_8$ solid solution series in order to determine the Ba/Sr ratio at which structure symmetry changed. After that, structure analysis was performed using their XRD patterns. The resultant crystal structures were checked by factor group analysis using the Raman spectra again.

## II. EXPERIMENTAL

### A. Synthesis

$Ba_xSr_{3-x}MgSi_2O_8$ polycrystalline samples were prepared by solid-state reaction of reagent grade alkaline–earth carbonates, magnesium carbonate hydroxide, and silica. A small amount of ammonium chloride was used as a flux. Stoichiometric amounts of the reagents and the flux were ground and mixed by ball milling with zirconia beads in 2-propanol for 4 h. The mixed powder was heated at 1100 °C for 4 h in air with an intermittent regrinding.

### B. Raman spectroscopy

Raman spectra were measured for the prepared samples at room temperature in backscattering geometry by a 3000 grooves $mm^{-1}$ grating monochromator and charge-coupled device detector system (RENISHAW, inVia Reflex system).

a)Author to whom correspondence should be addressed. Electronic mail: yonesaki@yamanashi.ac.jp



https://doi.org/10.1017/S0885715614000803 Published online by Cambridge University Press

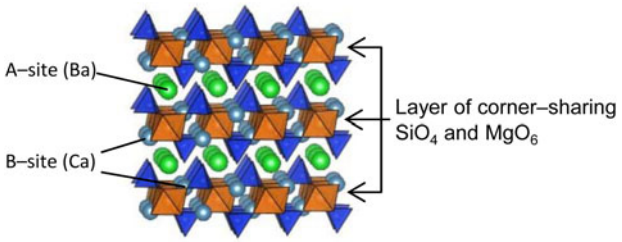



Figure 1. (Color online) Crystal structure of $BaCa_2MgSi_2O_8$ illustrated with $SiO_4$ tetrahedra and $MgO_6$ octahedra.

Samples were excited with the 488-nm line of a 50 mW Spectra–Physics Cyan™ Scientific CW laser. The laser beam was focused on a sample by a 50× objective lens. A spectral resolution was 0.5 $cm^{-1}$. The laser power was attenuated to 5 mW before the irradiation. The obtained data were used for checking the symmetries of $SiO_4$-derived vibrational modes.

### C. XRD analysis

The prepared samples were ground with mortar and pestle and investigated by XRD at room temperature with a Rigaku RINT-2200HFV diffractometer in a $2\theta$ range from 10° to 120° using Cu$K\alpha$ radiation ($\lambda = 1.5406$ Å, 40 kV, 30 mA). The obtained data were used for checking impurities and for structure refinement processes. Structure refinement was carried out with the XRD data collected with step-scanning mode at intervals of 0.05° or 0.02° $2\theta$. After the probable space group selection with the indexing program TREOR90 (Werner *et al.*, 1985), structure parameters were refined by the Rietveld method using the refinement program RIETAN–FP (Izumi and Momma, 2007). The influence of the Cu$K\alpha_2$ line was taken into calculation in the refinement processes. Pseudo-Voigt function was used to fit the peak profile. Figures of the crystal structure were drawn with VESTA developed by Momma and Izumi (2011).

## III. RESULTS

### A. Raman spectroscopy

Figure 2 shows the Raman spectra of the prepared solid-solution series. Intense peaks were confirmed at about 880, 400, 1000, and 550 $cm^{-1}$. Raman peaks at such high wavenumbers are attributed to the internal vibrations of certain atomic groups. In the present case, they corresponded to the four normal modes of $SiO_4$ tetrahedra: symmetric-stretching vibrations $\nu_1$, symmetric-bending vibrations $\nu_2$, asymmetric-stretching vibrations $\nu_3$, and asymmetric-bending vibrations $\nu_4$, respectively (Remy *et al.*, 1997). The Raman peaks below this region were because of the translational modes. In the $Ba_xSr_{3-x}MgSi_2O_8$ series, a systematic peak shift was seen for the $SiO_4$ internal vibrations in response to Ba/Sr replacement, which indicated that the crystal structure deformed continuously. It should be noted that some of the vibrational modes split or broadened for $x \geq 2.5$ ($\nu_2$ and $\nu_4$) and $< 0.5$ ($\nu_1$, $\nu_2$, and $\nu_4$). In both regions, translational modes also split. Such splits relate to the resolving of vibrational degeneracy associated with symmetry reduction. Therefore,

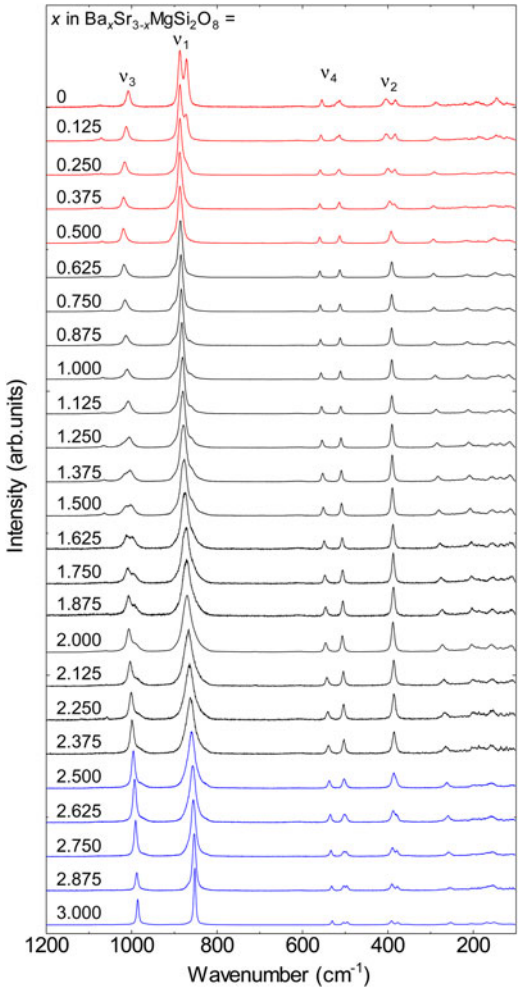



Figure 2. (Color online) Raman spectra for $Ba_xSr_{3-x}MgSi_2O_8$ solid solution series. $\nu_1$, $\nu_2$, $\nu_3$, and $\nu_4$ correspond to symmetric-stretching vibrations, symmetric-bending vibrations, asymmetric-stretching vibrations, and asymmetric-bending vibrations, respectively. Individual spectra are categorized with different color based on the splitting behaviors of each vibrational mode.

$Ba_xSr_{3-x}MgSi_2O_8$ series were categorized into three groups from the structural viewpoint: (i) $x \leq 0.5$, (ii) $2.5 > x > 0.5$, and (iii) $x \geq 2.5$.

### B. XRD analysis

Figure 3(a) shows the XRD patterns of the $Ba_xSr_{3-x}MgSi_2O_8$ samples. All the samples showed similar patterns, indicating their structural similarity. As for the samples of the Sr-rich group (i), all the diffraction peaks were successfully indexed with monoclinic cells of $a = 9.4$ Å, $b = 5.5$ Å, $c = 13.9$ Å, and $\beta = 90°$, while systematic absence of $h + k = 2n + 1$ was found. It is noteworthy that the *hkl* reflections having odd $l$ were extremely weak. Furthermore, they attenuated with increasing Ba-ratio. This attenuation was followed by the halved $c$ for $x > 0.5$. As for the samples of group (ii), most diffraction peaks were indexed with hexagonal cells of $a = 5.5$ and $c = 7.0$ Å, the volume of which was about four times smaller than the monoclinic cells of group (i). The other peaks observed for $x > 2$ were assigned to $BaMgSiO_4$. For the Ba-rich group (iii), the obtained patterns were similar to those of group (ii). However, careful observation identified


https://doi.org/10.1017/S0885715614000803 Published online by Cambridge University Press

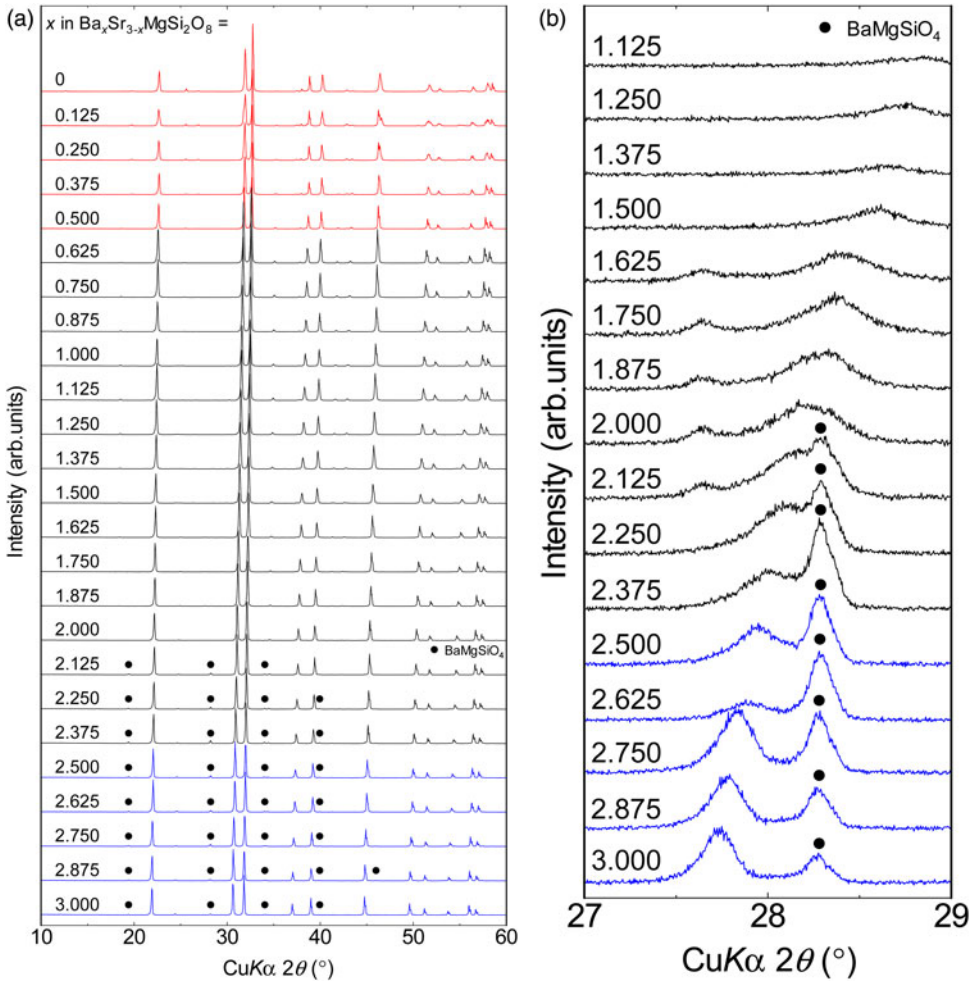



Figure 3. (Color online) (a) XRD patterns for $Ba_xSr_{3-x}MgSi_2O_8$ solid solution series. Individual patterns are categorized with different color based on the splitting behaviors of each vibrational mode (Figure 2). (b) Enlarged patterns of Figure 3(a).

another diffraction peak at 27.8° 2$\theta$ [Figure 3(b)], the intensity of which was below 0.2% of the highest. By involving the identified peak in the indexing process, hexagonal cells of $a = 9.7$ Å and $c = 7.2$ Å were derived. This cell is about $\sqrt{3} \times \sqrt{3} \times 1$ times larger than those of group (ii).

Structural refinement was performed based on the obtained unit-cell parameters and systematic absence. The approximate structures of $M_3MgSi_2O_8$ ($M$ = Ba, Sr, Ca) (Yonesaki *et al.*, 2008) were used as initial models. For the $BaMgSiO_4$ phase, only the scale factors, unit-cell parameters, and profile functions were refined. The refined cell and structure parameters are listed in Tables I and II. The obtained structure was checked by factor group analysis of the Raman spectra (Figure 4). As for group (ii), Raman peak numbers agreed with the calculated ones (1$\nu_1$, 1$\nu_2$, 2$\nu_3$, and 2$\nu_4$). Although those of the other compounds were less than the expected [2$\nu_1$, 4$\nu_2$, 6$\nu_3$, and 6$\nu_4$ for group (i) and 4$\nu_1$, 8$\nu_2$, 12$\nu_3$, and 12$\nu_4$ for group (iii)], it was due to the fact that the non-degenerated Raman peaks did not split enough for separation. Nevertheless, we can obtain important information on the structure of group (iii) from this analysis. For a group (iii) compound $Ba_3MgSi_2O_8$, two structure models have been proposed: $P\bar{3}m1$ ($Z = 1$) (Aitasalo *et al.*, 2007; Yonesaki *et al.*, 2009) and $P\bar{3}$ ($Z = 3$) models (Park *et al.*, 2009). There is a slight difference in $SiO_4$ orientation between them. The former model is identical to those of group (ii). All the $SiO_4$ tetrahedra point vertically to the layers. On the other hand, they tilt in the latter. From the Raman spectra measured in this study (Figure 2), the former model was excluded because at least two $\nu_2$ modes were present for the compounds of group (iii). If the $P\bar{3}m1$ ($Z = 1$) model were correct, only one $\nu_2$ mode would be observed [Figure 4(b)]. Iwata *et al.* (2009) showed the $SiO_4$ tilting with a split-atom model under the condition of $P\bar{3}m1$ ($Z$ = 1). However, the tilting was not statistical but regular, as is clear from the translational symmetry based on the characteristic diffraction peak at 27.8°. Therefore, the $P\bar{3}$ ($Z = 3$) model is reasonable for group (iii) compounds. As for $Sr_3MgSi_2O_8$ ($x = 0$), the refined structure may be approximate considering the high reliability index of $R_{wp}$. However, in this study, structural change caused by Ba/Sr replacement is discussed using this model. From the refined structure, it has been revealed that with increasing Ba ratio, $Ba_xSr_{3-x}MgSi_2O_8$ changes its space group in the following order: $C2$ ($Z = 4$), $P\bar{3}m1$ ($Z = 1$), and $P\bar{3}$ ($Z = 3$). The former change corresponds to the generation of threefold rotation axes and mirror planes in addition to the halved period in the layer-stacking direction. The latter change is


https://doi.org/10.1017/S0885715614000803 Published online by Cambridge University Press

TABLE I. Crystallographic data for $Ba_xSr_{3-x}MgSi_2O_8$ solid solutions.

| Empirical formula | $Sr_{3.000}MgSi_2O_8$ | $Ba_{0.125}Sr_{2.875}MgSi_2O_8$ | $Ba_{0.250}Sr_{2.750}MgSi_2O_8$ | $Ba_{0.375}Sr_{2.625}MgSi_2O_8$ | $Ba_{0.500}Sr_{2.500}MgSi_2O_8$ |
|---|---|---|---|---|---|
| Formula weight | 471.331 | 477.544 | 483.758 | 489.971 | 496.185 |
| Space group | *C*2(5) | *C*2(5) | *C*2(5) | *C*2(5) | *C*2(5) |
| Unit-cell parameters *a* (Å) | 9.449(3) | 9.452(1) | 9.463(1) | 9.474(1) | 9.485(1) |
| *b* (Å) | 5.453(1) | 5.4637(8) | 5.4690(6) | 5.4735(6) | 5.4765(6) |
| *c* (Å) | 13.871(4) | 13.886(2) | 13.898(2) | 13.913(1) | 13.931(1) |
| *β* (°) | 90.153(2) | 90.4453(8) | 90.2513(6) | 90.1012(7) | 90.011(6) |
| Volume (Å$^3$) | 714.9(3) | 717.1(2) | 719.3(1) | 721.5(1) | 723.7(1) |
| *Z* | 4 | 4 | 4 | 4 | 4 |
| Calculated density (g cm$^{-3}$) | 4.379 | 4.423 | 4.467 | 4.510 | 4.554 |
| $R_p$ (%) | 9.612 | 7.105 | 6.041 | 6.094 | 6.404 |
| $R_{wp}$ (%) | 13.345 | 9.474 | 8.564 | 8.866 | 9.375 |
| $R_I$ (%) | 3.105 | 1.433 | 1.147 | 1.395 | 1.521 |
| $R_F$ (%) | 2.561 | 1.069 | 1.108 | 1.406 | 2.003 |
| Goodness of fit | 2.070 | 1.412 | 1.240 | 1.235 | 1.295 |
| Empirical formula | $Ba_{0.625}Sr_{2.375}MgSi_2O_8$ | $Ba_{0.750}Sr_{2.250}MgSi_2O_8$ | $Ba_{0.875}Sr_{2.125}MgSi_2O_8$ | $Ba_{1.000}Sr_{2.000}MgSi_2O_8$ | $Ba_{1.125}Sr_{1.875}MgSi_2O_8$ |
| Formula weight | 502.398 | 508.611 | 514.825 | 521.038 | 527.251 |
| Space group | $P\bar{3}m1$(164) | $P\bar{3}m1$(164) | $P\bar{3}m1$(164) | $P\bar{3}m1$(164) | $P\bar{3}m1$(164) |
| Unit-cell parameters *a* (Å) | 5.4840(8) | 5.489(1) | 5.494(1) | 5.498(1) | 5.502(1) |
| *c* (Å) | 6.9806(8) | 6.9933(9) | 7.006(1) | 7.0179(9) | 7.030(1) |
| Volume (Å$^3$) | 181.81(4) | 182.51(5) | 183.20(5) | 183.77(5) | 184.33(7) |
| *Z* | 1 | 1 | 1 | 1 | 1 |
| Calculated density (g cm$^{-3}$) | 4.589 | 4.627 | 4.666 | 4.708 | 4.750 |
| $R_p$ (%) | 5.410 | 5.480 | 5.947 | 6.100 | 5.815 |
| $R_{wp}$ (%) | 7.907 | 8.036 | 8.808 | 8.987 | 9.153 |
| $R_I$ (%) | 1.525 | 1.713 | 1.523 | 1.932 | 1.312 |
| $R_F$ (%) | 1.271 | 1.284 | 1.308 | 1.477 | 0.964 |
| Goodness of fit | 1.362 | 1.364 | 1.336 | 1.334 | 1.498 |
| Empirical formula | $Ba_{1.250}Sr_{1.750}MgSi_2O_8$ | $Ba_{1.375}Sr_{1.625}MgSi_2O_8$ | $Ba_{1.500}Sr_{1.500}MgSi_2O_8$ | $Ba_{1.625}Sr_{1.375}MgSi_2O_8$ | $Ba_{1.750}Sr_{1.250}MgSi_2O_8$ |
| Formula weight | 533.465 | 539.678 | 545.892 | 552.105 | 558.318 |
| Space group | $P\bar{3}m1$(164) | $P\bar{3}m1$(164) | $P\bar{3}m1$(164) | $P\bar{3}m1$(164) | $P\bar{3}m1$(164) |
| Unit-cell parameters *a* (Å) | 5.513(1) | 5.520(1) | 5.526(1) | 5.532(1) | 5.539(1) |
| *c* (Å) | 7.051(1) | 7.067(1) | 7.082(1) | 7.096(1) | 7.114(1) |
| Volume (Å$^3$) | 185.62(7) | 186.52(7) | 187.32(8) | 188.11(6) | 189.08(6) |
| *Z* | 1 | 1 | 1 | 1 | 1 |
| Calculated density (g cm$^{-3}$) | 4.772 | 4.804 | 4.839 | 4.874 | 4.903 |
| $R_p$ (%) | 6.086 | 6.089 | 6.491 | 6.389 | 5.959 |
| $R_{wp}$ (%) | 9.428 | 9.400 | 9.989 | 9.311 | 9.317 |
| $R_I$ (%) | 1.822 | 1.621 | 2.107 | 1.723 | 1.425 |
| $R_F$ (%) | 1.383 | 1.233 | 1.464 | 1.407 | 1.376 |
| Goodness of fit | 1.518 | 1.490 | 1.463 | 1.344 | 1.278 |
| Empirical formula | $Ba_{1.875}Sr_{1.125}MgSi_2O_8$ | $Ba_{2.000}Sr_{1.000}MgSi_2O_8$ | $Ba_{2.125}Sr_{0.875}MgSi_2O_8$ | $Ba_{2.250}Sr_{0.750}MgSi_2O_8$ | $Ba_{2.375}Sr_{0.625}MgSi_2O_8$ |
| Formula weight | 564.532 | 570.745 | 576.958 | 583.172 | 589.385 |
| Space group | $P\bar{3}m1$(164) | $P\bar{3}m1$(164) | $P\bar{3}m1$(164) | $P\bar{3}m1$(164) | $P\bar{3}m1$(164) |
| Unit-cell parameters *a* (Å) | 5.546(1) | 5.5532(9) | 5.5606(9) | 5.566(1) | 5.573(1) |
| *c* (Å) | 7.129(1) | 7.1460(9) | 7.1617(8) | 7.176(1) | 7.1909(9) |
| Volume (Å$^3$) | 189.91(6) | 190.85(5) | 191.78(5) | 192.60(6) | 193.46(5) |
| *Z* | 1 | 1 | 1 | 1 | 1 |
| Calculated density (g cm$^{-3}$) | 4.936 | 4.966 | 4.996 | 5.028 | 5.059 |
| $R_p$ (%) | 6.294 | 6.290 | 6.396 | 6.445 | 6.374 |
| $R_{wp}$ (%) | 9.568 | 9.496 | 9.309 | 9.516 | 9.568 |
| $R_I$ (%) | 1.604 | 1.609 | 1.410 | 1.903 | 1.602 |
| $R_F$ (%) | 1.379 | 1.653 | 1.187 | 1.463 | 1.308 |
| Goodness of fit | 1.348 | 1.314 | 1.282 | 1.294 | 1.300 |
| Empirical formula | $Ba_{2.500}Sr_{0.500}MgSi_2O_8$ | $Ba_{2.625}Sr_{0.375}MgSi_2O_8$ | $Ba_{2.750}Sr_{0.250}MgSi_2O_8$ | $Ba_{2.875}Sr_{0.125}MgSi_2O_8$ | $Ba_{3.000}MgSi_2O_8$ |
| Formula weight | 595.599 | 601.812 | 608.025 | 614.239 | 620.452 |
| Space group | $P\bar{3}$ (147) | $P\bar{3}$ (147) | $P\bar{3}$ (147) | $P\bar{3}$ (147) | $P\bar{3}$ (147) |
| Unit-cell parameters *a* (Å) | 9.666(2) | 9.679(2) | 9.689(1) | 9.701(1) | 9.7180(7) |
| *c* (Å) | 7.2076(9) | 7.2231(9) | 7.2380(8) | 7.2535(8) | 7.2715(4) |
| Volume (Å$^3$) | 583.2(2) | 586.0(2) | 588.5(1) | 591.2(1) | 594.72(7) |

*Continued*



https://doi.org/10.1017/S0885715614000803 Published online by Cambridge University Press

TABLE I. Continued

| Empirical formula | $Ba_{2.500}Sr_{0.500}MgSi_2O_8$ | $Ba_{2.625}Sr_{0.375}MgSi_2O_8$ | $Ba_{2.750}Sr_{0.250}MgSi_2O_8$ | $Ba_{2.875}Sr_{0.125}MgSi_2O_8$ | $Ba_{3.000}MgSi_2O_8$ |
|---|---|---|---|---|---|
| $Z$ | 3 | 3 | 3 | 3 | 3 |
| Calculated density (g cm$^{-3}$) | 5.087 | 5.116 | 5.146 | 5.175 | 5.197 |
| $R_p$ (%) | 6.557 | 6.594 | 6.904 | 6.806 | 7.112 |
| $R_{wp}$ (%) | 9.769 | 9.748 | 10.267 | 10.324 | 10.538 |
| $R_I$ (%) | 1.636 | 2.230 | 2.504 | 1.808 | 1.972 |
| $R_F$ (%) | 1.754 | 1.953 | 2.165 | 2.074 | 2.186 |
| Goodness of fit | 1.260 | 1.299 | 1.278 | 1.256 | 1.363 |

TABLE II. Atomic coordinates and isotropic displacement parameters for $Ba_xSr_{3-x}MgSi_2O_8$.

| Group (i) | | | | | |
|---|---|---|---|---|---|
| $Sr_3MgSi_2O_8$ ($x = 0$) | | | | | |
| | $g$ | $x$ | $y$ | $z$ | $B_{iso}$ (Å$^2$) |
| $Sr_1$ | 1 | 0 | 0.062(3) | 1/2 | 1.5(3) |
| $Sr_2$ | 1 | 0 | 0 | 0 | 3.4(4) |
| $Sr_3$ | 1 | 0.1762(8) | 0.519(3) | 0.1629(5) | 1.4(2) |
| $Sr_4$ | 1 | 0.3436(7) | 0.013(3) | 0.3379(4) | 0.2(1) |
| Mg | 1 | −0.004(3) | 0.045(4) | 0.248(2) | 0.5 |
| $Si_1$ | 1 | 0.167(2) | 0.524(5) | 0.386(1) | 0.7(1) |
| $Si_2$ | 1 | 0.327(2) | 0.024(5) | 0.113(1) | $B(Si_1)$ |
| $O_1$ | 1 | 0.095(7) | 0.257(9) | 0.331(3) | 0.6(2) |
| $O_2$ | 1 | 0.164(3) | −0.01(1) | 0.648(2) | $B(O_1)$ |
| $O_3$ | 1 | 0.192(3) | 0.527(7) | 0.488(2) | $B(O_1)$ |
| $O_4$ | 1 | 0.180(4) | 0.00(1) | 0.159(3) | $B(O_1)$ |
| $O_5$ | 1 | 0.359(4) | 0.053(6) | 0.002(2) | $B(O_1)$ |
| $O_6$ | 1 | 0.432(5) | 0.747(7) | 0.123(2) | $B(O_1)$ |
| $O_7$ | 1 | 0.420(6) | 0.216(7) | 0.170(3) | $B(O_1)$ |
| $O_8$ | 1 | 0.605(6) | 0.232(9) | 0.329(2) | $B(O_1)$ |
| $Ba_{0.125}Sr_{2.875}MgSi_2O_8$ ($x = 0.125$) | | | | | |
| $Ba_1/Sr_1$ | 0.087(9)/1−$g$(Ba$_1$) | 0 | 0.079(1) | 1/2 | 0.4(2) |
| $Ba_2/Sr_2$ | 0.25−$g$(Ba$_1$)/0.75 + $g$(Ba$_1$) | 0 | 0 | 0 | 2.3(2) |
| $Sr_3$ | 1 | 0.1766(5) | 0.549(2) | 0.3354(3) | 0.9(1) |
| $Sr_4$ | 1 | 0.3347(5) | 0.025(2) | 0.1646(3) | 0.3(1) |
| Mg | 1 | −0.002(2) | 0.035(8) | 0.251(2) | 0.6(2) |
| $Si_1$ | 1 | 0.164(1) | 0.530(6) | 0.114(1) | 0.37(7) |
| $Si_2$ | 1 | 0.337(1) | 0.048(6) | 0.386(1) | $B(Si_1)$ |
| $O_1$ | 1 | 0.075(4) | 0.316(9) | 0.672(2) | 0.5(1) |
| $O_2$ | 1 | 0.078(4) | 0.271(7) | 0.148(2) | $B(O_1)$ |
| $O_3$ | 1 | 0.162(2) | 0.486(7) | 0.501(2) | $B(O_1)$ |
| $O_4$ | 1 | 0.195(2) | 0.058(9) | 0.337(2) | $B(O_1)$ |
| $O_5$ | 1 | 0.182(3) | 0.600(7) | 0.006(2) | $B(O_1)$ |
| $O_6$ | 1 | 0.329(3) | 0.509(9) | 0.162(2) | $B(O_1)$ |
| $O_7$ | 1 | 0.424(3) | 0.284(6) | 0.366(2) | $B(O_1)$ |
| $O_8$ | 1 | 0.581(3) | 0.242(8) | 0.167(2) | $B(O_1)$ |
| $Ba_{0.250}Sr_{2.750}MgSi_2O_8$ ($x = 0.250$) | | | | | |
| $Ba_1/Sr_1$ | 0.234(8)/1−$g$(Ba$_1$) | 0 | 0.066(1) | 1/2 | 1.3(2) |
| $Ba_2/Sr_2$ | 0.5−$g$(Ba$_1$)/0.5 + $g$(Ba$_1$) | 0 | 0 | 0 | 1.4(2) |
| $Sr_3$ | 1 | 0.1693(6) | 0.541(3) | 0.3336(5) | 0.7(1) |
| $Sr_4$ | 1 | 0.3303(6) | 0.021(3) | 0.1663(5) | 0.3(1) |
| Mg | 1 | 0.005(3) | 0.026(6) | 0.254(1) | 0.5(2) |
| $Si_1$ | 1 | 0.162(2) | 0.529(7) | 0.114(1) | 0.38(8) |
| $Si_2$ | 1 | 0.334(2) | 0.036(7) | 0.388(1) | $B(Si_1)$ |
| $O_1$ | 1 | 0.070(3) | 0.303(5) | 0.672(2) | 0.3(1) |
| $O_2$ | 1 | 0.082(4) | 0.267(7) | 0.155(2) | $B(O_1)$ |
| $O_3$ | 1 | 0.155(2) | 0.496(6) | 0.502(2) | $B(O_1)$ |
| $O_4$ | 1 | 0.196(2) | 0.058(6) | 0.343(1) | $B(O_1)$ |
| $O_5$ | 1 | 0.182(2) | 0.582(7) | 0.001(2) | $B(O_1)$ |
| $O_6$ | 1 | 0.340(3) | 0.518(8) | 0.165(2) | $B(O_1)$ |
| $O_7$ | 1 | 0.426(3) | 0.281(5) | 0.364(2) | $B(O_1)$ |
| $O_8$ | 1 | 0.593(4) | 0.249(6) | 0.164(2) | $B(O_1)$ |

*Continued*


https://doi.org/10.1017/S0885715614000803 Published online by Cambridge University Press

TABLE II. Continued

| Group (i) | | | | | |
|---|---|---|---|---|---|
| | $g$ | $x$ | $y$ | $z$ | $B_{iso}$ (Å$^2$) |
| $Ba_{0.375}Sr_{2.625}MgSi_2O_8$ ($x = 0.375$) | | | | | |
| $Ba_1/Sr_1$ | 0.374(8)/1–$g$($Ba_1$) | 0 | 0.045(1) | 1/2 | 1.4(3) |
| $Ba_2/Sr_2$ | 0.75–$g$($Ba_1$)/0.25 + $g$($Ba_1$) | 0 | 0 | 0 | 1.5(3) |
| $Sr_3$ | 1 | 0.1693(8) | 0.529(3) | 0.3323(6) | 0.5(1) |
| $Sr_4$ | 1 | 0.3322(7) | 0.017(3) | 0.1673(6) | 0.3(1) |
| Mg | 1 | 0.008(2) | 0.022(9) | 0.252(2) | 0.4(2) |
| $Si_1$ | 1 | 0.163(2) | 0.528(5) | 0.113(2) | 0.19(9) |
| $Si_2$ | 1 | 0.331(2) | 0.032(5) | 0.387(2) | $B$($Si_1$) |
| $O_1$ | 1 | 0.071(5) | 0.283(7) | 0.670(2) | 0.2(1) |
| $O_2$ | 1 | 0.091(6) | 0.277(9) | 0.163(2) | $B$($O_1$) |
| $O_3$ | 1 | 0.153(3) | 0.502(7) | 0.499(2) | $B$($O_1$) |
| $O_4$ | 1 | 0.191(3) | 0.04(1) | 0.343(2) | $B$($O_1$) |
| $O_5$ | 1 | 0.177(3) | 0.566(7) | 0.001(2) | $B$($O_1$) |
| $O_6$ | 1 | 0.336(4) | 0.52(1) | 0.160(3) | $B$($O_1$) |
| $O_7$ | 1 | 0.426(4) | 0.270(6) | 0.361(2) | $B$($O_1$) |
| $O_8$ | 1 | 0.600(6) | 0.242(7) | 0.162(3) | $B$($O_1$) |
| $Ba_{0.500}Sr_{2.500}MgSi_2O_8$ ($x = 0.500$) | | | | | |
| $Ba_1/Sr_1$ | 0.48(9)/1–$g$($Ba_1$) | 0 | 0.015(4) | 1/2 | 1.9(3) |
| $Ba_2/Sr_2$ | 1–$g$($Ba_1$)/$g$($Ba_1$) | 0 | 0 | 0 | 1.0(3) |
| $Sr_3$ | 1 | 0.168(2) | 0.514(5) | 0.3321(8) | 0.5(2) |
| $Sr_4$ | 1 | 0.335(2) | 0.009(4) | 0.1688(8) | 0.5(2) |
| Mg | 1 | −0.001(5) | 0.004(8) | 0.245(2) | 0.2(2) |
| $Si_1$ | 1 | 0.161(4) | 0.504(7) | 0.113(2) | 0.38(9) |
| $Si_2$ | 1 | 0.329(4) | 0.007(6) | 0.387(2) | $B$($Si_1$) |
| $O_1$ | 1 | 0.08(1) | 0.30(2) | 0.669(6) | 0.2(2) |
| $O_2$ | 1 | 0.09(2) | 0.29(3) | 0.162(5) | $B$($O_1$) |
| $O_3$ | 1 | 0.168(8) | 0.48(2) | 0.501(4) | $B$($O_1$) |
| $O_4$ | 1 | 0.173(9) | 0.03(3) | 0.33(1) | $B$($O_1$) |
| $O_5$ | 1 | 0.187(8) | 0.53(1) | −0.001(4) | $B$($O_1$) |
| $O_6$ | 1 | 0.325(9) | 0.53(5) | 0.15(1) | $B$($O_1$) |
| $O_7$ | 1 | 0.42(2) | 0.27(2) | 0.349(6) | $B$($O_1$) |
| $O_8$ | 1 | 0.59(2) | 0.25(3) | 0.151(7) | $B$($O_1$) |
| Group (ii) | | | | | |
| $Ba_{0.625}Sr_{2.375}MgSi_2O_8$ ($x = 0.625$) | | | | | |
| $Ba_1/Sr_1$ | 0.030(5)/1–$g$($Ba_1$) | 1/3 | 2/3 | 0.6624(2) | 0.61(5) |
| $Ba_2/Sr_2$ | 0.625–2 g($Ba_1$)/0.375 + 2 g($Ba_1$) | 0 | 0 | 0 | 1.00(6) |
| Mg | 1 | 0 | 0 | 1/2 | 0.6(2) |
| Si | 1 | 1/3 | 2/3 | 0.2259(5) | 0.39(8) |
| $O_1$ | 1 | 0.1749(8) | –$x$($O_1$) | 0.3179(7) | 0.91(8) |
| $O_2$ | 1 | 1/3 | 2/3 | 0.000(1) | $B$($O_1$) |
| $Ba_{0.750}Sr_{2.250}MgSi_2O_8$ ($x = 0.750$) | | | | | |
| $Ba_1/Sr_1$ | 0.042(5)/1–$g$($Ba_1$) | 1/3 | 2/3 | 0.6628(2) | 0.63(5) |
| $Ba_2/Sr_2$ | 0.75–2 g($Ba_1$)/0.25 + 2 g($Ba_1$) | 0 | 0 | 0 | 0.99(7) |
| Mg | 1 | 0 | 0 | 1/2 | 0.6(2) |
| Si | 1 | 1/3 | 2/3 | 0.2265(5) | 0.34(8) |
| $O_1$ | 1 | 0.1758(8) | –$x$($O_1$) | 0.3190(7) | 0.83(9) |
| $O_2$ | 1 | 1/3 | 2/3 | 0.000(1) | $B$($O_1$) |
| $Ba_{0.875}Sr_{2.125}MgSi_2O_8$ ($x = 0.875$) | | | | | |
| $Ba_1/Sr_1$ | 0.056(6)/1–$g$($Ba_1$) | 1/3 | 2/3 | 0.6633(3) | 0.58(7) |
| $Ba_2/Sr_2$ | 0.875–2 g($Ba_1$)/0.125 + 2 g($Ba_1$) | 0 | 0 | 0 | 1.03(8) |
| Mg | 1 | 0 | 0 | 1/2 | 0.2(2) |
| Si | 1 | 1/3 | 2/3 | 0.2285(6) | 0.5(1) |
| $O_1$ | 1 | 0.1765(9) | –$x$($O_1$) | 0.3187(9) | 0.9(1) |
| $O_2$ | 1 | 1/3 | 2/3 | 0.001(1) | $B$($O_1$) |
| $Ba_{1.000}Sr_{2.000}MgSi_2O_8$ ($x = 1.000$) | | | | | |
| $Ba_1/Sr_1$ | 0.087(6)/1–$g$($Ba_1$) | 1/3 | 2/3 | 0.6640(3) | 0.51(6) |
| $Ba_2/Sr_2$ | 1–2 g($Ba_1$)/2 g($Ba_1$) | 0 | 0 | 0 | 0.93(7) |
| Mg | 1 | 0 | 0 | 1/2 | 0.6(2) |
| Si | 1 | 1/3 | 2/3 | 0.2277(6) | 0.21(9) |

*Continued*


https://doi.org/10.1017/S0885715614000803 Published online by Cambridge University Press

TABLE II. Continued

| Group (ii) | | | | | |
|---|---|---|---|---|---|
| $O_1$ | 1 | 0.176(1) | $-x(O_1)$ | 0.3184(9) | 0.7(1) |
| $O_2$ | 1 | 1/3 | 2/3 | 0.001(1) | $B(O_1)$ |
| $Ba_{1.125}Sr_{1.875}MgSi_2O_8$ ($x = 1.125$) | | | | | |
| $Ba_1/Sr_1$ | $0.136(7)/1-g(Ba_1)$ | 1/3 | 2/3 | 0.6638(3) | 0.70(7) |
| $Ba_2/Sr_2$ | $1.125-2\ g(Ba_1)/-0.125+2\ g(Ba_1)$ | 0 | 0 | 0 | 0.74(8) |
| Mg | 1 | 0 | 0 | 1/2 | 0.7(2) |
| Si | 1 | 1/3 | 2/3 | 0.2287(6) | 0.3(1) |
| $O_1$ | 1 | 0.173(1) | $-x(O_1)$ | 0.321(1) | 0.8(1) |
| $O_2$ | 1 | 1/3 | 2/3 | 0.003(1) | $B(O_1)$ |
| $Ba_{1.250}Sr_{1.750}MgSi_2O_8$ ($x = 1.250$) | | | | | |
| $Ba_1/Sr_1$ | $0.174(7)/1-g(Ba_1)$ | 1/3 | 2/3 | 0.6647(3) | 0.62(8) |
| $Ba_2/Sr_2$ | $1.25-2\ g(Ba_1)/-0.25+2\ g(Ba_1)$ | 0 | 0 | 0 | 0.74(9) |
| Mg | 1 | 0 | 0 | 1/2 | 0.6(2) |
| Si | 1 | 1/3 | 2/3 | 0.2300(7) | 0.3(1) |
| $O_1$ | 1 | 0.175(1) | $-x(O_1)$ | 0.321(1) | 0.7(1) |
| $O_2$ | 1 | 1/3 | 2/3 | 0.004(1) | $B(O_1)$ |
| $Ba_{1.375}Sr_{1.625}MgSi_2O_8$ ($x = 1.375$) | | | | | |
| $Ba_1/Sr_1$ | $0.234(8)/1-g(Ba_1)$ | 1/3 | 2/3 | 0.6654(3) | 0.66(7) |
| $Ba_2/Sr_2$ | $1.375-2\ g(Ba_1)/-0.375+2\ g(Ba_1)$ | 0 | 0 | 0 | 0.69(9) |
| Mg | 1 | 0 | 0 | 1/2 | 0.4(2) |
| Si | 1 | 1/3 | 2/3 | 0.2305(7) | 0.3(1) |
| $O_1$ | 1 | 0.175(1) | $-x(O_1)$ | 0.322(1) | 0.9(1) |
| $O_2$ | 1 | 1/3 | 2/3 | 0.006(2) | $B(O_1)$ |
| $Ba_{1.500}Sr_{1.500}MgSi_2O_8$ ($x = 1.500$) | | | | | |
| $Ba_1/Sr_1$ | $0.294(9)/1-g(Ba_1)$ | 1/3 | 2/3 | 0.6664(3) | 0.67(7) |
| $Ba_2/Sr_2$ | $1.5-2\ g(Ba_1)/-0.5+2\ g(Ba_1)$ | 0 | 0 | 0 | 0.6(1) |
| Mg | 1 | 0 | 0 | 1/2 | 0.8(3) |
| Si | 1 | 1/3 | 2/3 | 0.2296(8) | 0.2(1) |
| $O_1$ | 1 | 0.174(1) | $-x(O_1)$ | 0.321(1) | 0.7(1) |
| $O_2$ | 1 | 1/3 | 2/3 | 0.007(2) | $B(O_1)$ |
| $Ba_{1.625}Sr_{1.375}MgSi_2O_8$ ($x = 1.625$) | | | | | |
| $Ba_1/Sr_1$ | $0.338(8)/1-g(Ba_1)$ | 1/3 | 2/3 | 0.6674(3) | 0.63(7) |
| $Ba_2/Sr_2$ | $1.625-2\ g(Ba_1)/-0.625+2\ g(Ba_1)$ | 0 | 0 | 0 | 0.72(8) |
| Mg | 1 | 0 | 0 | 1/2 | 0.4(2) |
| Si | 1 | 1/3 | 2/3 | 0.2319(8) | 0.5(1) |
| $O_1$ | 1 | 0.173(1) | $-x(O_1)$ | 0.320(1) | 0.7(1) |
| $O_2$ | 1 | 1/3 | 2/3 | 0.006(2) | $B(O_1)$ |
| $Ba_{1.750}Sr_{1.250}MgSi_2O_8$ ($x = 1.750$) | | | | | |
| $Ba_1/Sr_1$ | $0.410(8)/1-g(Ba_1)$ | 1/3 | 2/3 | 0.6679(3) | 0.66(7) |
| $Ba_2/Sr_2$ | $1.75-2\ g(Ba_1)/-0.75+2\ g(Ba_1)$ | 0 | 0 | 0 | 0.71(9) |
| Mg | 1 | 0 | 0 | 1/2 | 0.8(2) |
| Si | 1 | 1/3 | 2/3 | 0.2311(7) | 0.4(1) |
| $O_1$ | 1 | 0.174(1) | $-x(O_1)$ | 0.3218(9) | 0.9(1) |
| $O_2$ | 1 | 1/3 | 2/3 | 0.010(1) | $B(O_1)$ |
| $Ba_{1.875}Sr_{1.125}MgSi_2O_8$ ($x = 1.875$) | | | | | |
| $Ba_1/Sr_1$ | $0.476(8)/1-g(Ba_1)$ | 1/3 | 2/3 | 0.6686(3) | 0.67(7) |
| $Ba_2/Sr_2$ | $1.875-2\ g(Ba_1)/-0.875+2\ g(Ba_1)$ | 0 | 0 | 0 | 0.64(9) |
| Mg | 1 | 0 | 0 | 1/2 | 0.5(3) |
| Si | 1 | 1/3 | 2/3 | 0.2321(8) | 0.6(1) |
| $O_1$ | 1 | 0.171(2) | $-x(O_1)$ | 0.322(1) | 0.8(1) |
| $O_2$ | 1 | 1/3 | 2/3 | 0.011(2) | $B(O_1)$ |
| $Ba_{2.000}Sr_{1.000}MgSi_2O_8$ ($x = 2.000$) | | | | | |
| $Ba_1/Sr_1$ | $0.51(1)/1-g(Ba_1)$ | 1/3 | 2/3 | 0.6703(3) | 0.49(8) |
| $Ba_2/Sr_2$ | $2-2\ g(Ba_1)/-1+2\ g(Ba_1)$ | 0 | 0 | 0 | 0.8(1) |
| Mg | 1 | 0 | 0 | 1/2 | 0.7(3) |
| Si | 1 | 1/3 | 2/3 | 0.2326(8) | 0.3(1) |
| $O_1$ | 1 | 0.176(2) | $-x(O_1)$ | 0.322(1) | 0.9(1) |
| $O_2$ | 1 | 1/3 | 2/3 | 0.010(2) | $B(O_1)$ |
| $Ba_{2.125}Sr_{0.875}MgSi_2O_8$ ($x = 2.125$) | | | | | |
| $Ba_1/Sr_1$ | $0.581(9)/1-g(Ba_1)$ | 1/3 | 2/3 | 0.6709(3) | 0.48(7) |
| $Ba_2/Sr_2$ | $2.125-2\ g(Ba_1)/-1.125+2\ g(Ba_1)$ | 0 | 0 | 0 | 0.8(1) |
| Mg | 1 | 0 | 0 | 1/2 | 0.4(3) |

*Continued*


https://doi.org/10.1017/S0885715614000803 Published online by Cambridge University Press

TABLE II. Continued

| | | | | | |
|---|---|---|---|---|---|
| Group (ii) | | | | | |
| Si | 1 | 1/3 | 2/3 | 0.2338(9) | 0.4(1) |
| $O_1$ | 1 | 0.172(2) | $-x(O_1)$ | 0.321(1) | 1.0(1) |
| $O_2$ | 1 | 1/3 | 2/3 | 0.013(2) | $B(O_1)$ |
| $Ba_{2.250}Sr_{0.750}MgSi_2O_8$ ($x = 2.250$) | | | | | |
| $Ba_1/Sr_1$ | 0.64(1)/1–$g(Ba_1)$ | 1/3 | 2/3 | 0.6716(3) | 0.41(8) |
| $Ba_2/Sr_2$ | 2.25–2 $g(Ba_1)$/ − 1.25 + 2 $g(Ba_1)$ | 0 | 0 | 0 | 0.9(1) |
| Mg | 1 | 0 | 0 | 1/2 | 0.6(3) |
| Si | 1 | 1/3 | 2/3 | 0.233(1) | 0.3(1) |
| $O_1$ | 1 | 0.172(2) | $-x(O_1)$ | 0.322(1) | 1.0(1) |
| $O_2$ | 1 | 1/3 | 2/3 | 0.015(2) | $B(O_1)$ |
| $Ba_{2.375}Sr_{0.625}MgSi_2O_8$ ($x = 2.375$) | | | | | |
| $Ba_1/Sr_1$ | 0.70(1)/1–$g(Ba_1)$ | 1/3 | 2/3 | 0.6727(4) | 0.45(9) |
| $Ba_2/Sr_2$ | 2.375–2 $g(Ba_1)$/ − 1.375 + 2 $g(Ba_1)$ | 0 | 0 | 0 | 0.9(1) |
| Mg | 1 | 0 | 0 | 1/2 | 0.9(3) |
| Si | 1 | 1/3 | 2/3 | 0.234(1) | 0.5(2) |
| $O_1$ | 1 | 0.177(2) | $-x(O_1)$ | 0.322(1) | 1.0(1) |
| $O_2$ | 1 | 1/3 | 2/3 | 0.015(2) | $B(O_1)$ |
| Group (iii) | | | | | |
| $Ba_{2.500}Sr_{0.500}MgSi_2O_8$ ($x = 2.500$) | | | | | |
| $Ba_1/Sr_1$ | 0.8125 + 0.5 $g(Sr_2)$/0.1875–0.5 g(Sr2) | 0.333(4) | 0.332(3) | 0.1743(4) | 0.56(7) |
| $Ba_2/Sr_2$ | 1–$g(Sr_2)$/0.07(3) | 1/3 | 2/3 | 0.501(3) | 0.7 (1) |
| $Ba_3/Sr_3$ | 1–$g(Sr_2)/g(Sr_2)$ | 0 | 0 | 1/2 | $B(Ba_2/Sr_2)$ |
| $Mg_1$ | 1 | 1/3 | 2/3 | 0.00(1) | 0.7(3) |
| $Mg_2$ | 1 | 0 | 0 | 0 | $B(Mg_1)$ |
| Si | 1 | 0.33(1) | −0.003(5) | 0.265(1) | 0.5(2) |
| $O_1$ | 1 | 0.00(1) | 0.17(2) | 0.17(1) | 0.8(2) |
| $O_2$ | 1 | 0.15(1) | 0.48(1) | 0.188(8) | $B(O_1)$ |
| $O_3$ | 1 | 0.354(9) | 0.023(7) | 0.480(2) | $B(O_1)$ |
| $O_4$ | 1 | 0.49(2) | 0.15(1) | 0.169(9) | $B(O_1)$ |
| $Ba_{2.625}Sr_{0.375}MgSi_2O_8$ ($x = 2.625$) | | | | | |
| $Ba_1/Sr_1$ | 0.8125 + 0.5 $g(Sr_2)$/0.1875–0.5 g(Sr2) | 0.333(3) | 0.332(3) | 0.1753(4) | 0.61(6) |
| $Ba_2/Sr_2$ | 1–$g(Sr_2)$/0.04(3) | 1/3 | 2/3 | 0.505(1) | 0.77(9) |
| $Ba_3/Sr_3$ | 1–$g(Sr_2)/g(Sr_2)$ | 0 | 0 | 1/2 | $B(Ba_2/Sr_2)$ |
| $Mg_1$ | 1 | 1/3 | 2/3 | 0.005(6) | 0.3(2) |
| $Mg_2$ | 1 | 0 | 0 | 0 | $B(Mg_1)$ |
| Si | 1 | 0.33(1) | 0.003(3) | 0.259(1) | 0.4(2) |
| $O_1$ | 1 | 0.00(2) | 0.16(1) | 0.17(2) | 0.7(2) |
| $O_2$ | 1 | 0.15(2) | 0.48(2) | 0.18(1) | $B(O_1)$ |
| $O_3$ | 1 | 0.349(7) | 0.032(3) | 0.483(2) | $B(O_1)$ |
| $O_4$ | 1 | 0.50(2) | 0.17(2) | 0.17(1) | $B(O_1)$ |
| $Ba_{2.750}Sr_{0.250}MgSi_2O_8$ ($x = 2.750$) | | | | | |
| $Ba_1/Sr_1$ | 0.875 + 0.5 $g(Sr_2)$/0.125–0.5 $g(Sr_2)$ | 0.332(2) | 0.332(2) | 0.1759(4) | 0.39(6) |
| $Ba_2/Sr_2$ | 1–$g(Sr_2)$/0.02(2) | 1/3 | 2/3 | 0.503(2) | 0.8(1) |
| $Ba_3/Sr_3$ | 1–$g(Sr_2)/g(Sr_2)$ | 0 | 0 | 1/2 | $B(Ba_2/Sr_2)$ |
| $Mg_1$ | 1 | 1/3 | 2/3 | −0.004(9) | 0.6(3) |
| $Mg_2$ | 1 | 0 | 0 | 0 | $B(Mg_1)$ |
| Si | 1 | 0.336(6) | 0.009(3) | 0.260(1) | 0.3(2) |
| $O_1$ | 1 | 0.00(4) | 0.16(2) | 0.166(8) | 1.0(2) |
| $O_2$ | 1 | 0.15(2) | 0.48(2) | 0.196(5) | $B(O_1)$ |
| $O_3$ | 1 | 0.361(6) | 0.025(6) | 0.477(2) | $B(O_1)$ |
| $O_4$ | 1 | 0.49(2) | 0.16(2) | 0.160(7) | $B(O_1)$ |
| $Ba_{2.875}Sr_{0.125}MgSi_2O_8$ ($x = 2.875$) | | | | | |
| $Ba_1/Sr_1$ | 0.9375 + 0.333 $g(Sr_2)$ + 0.167 $g(Sr_3)$/ 0.0625–0.333 $g(Sr_2)$ − 0.167 $g(Sr_3)$ | 0.333(1) | 0.333(1) | 0.1772(3) | 0.41(5) |
| $Ba_2/Sr_2$ | 1–$g(Sr_2)$/0.01(6) | 1/3 | 2/3 | 0.505(2) | 0.82(8) |
| $Ba_3/Sr_3$ | 1–$g(Sr_3)$/0.12(9) | 0 | 0 | 1/2 | $B(Ba_2/Sr_2)$ |
| $Mg_1$ | 1 | 1/3 | 2/3 | 0.010(8) | 0.6(3) |
| $Mg_2$ | 1 | 0 | 0 | 0 | $B(Mg_1)$ |
| Si | 1 | 0.339(5) | 0.008(3) | 0.261(1) | 0.4(2) |
| $O_1$ | 1 | 0.00(2) | 0.15(1) | 0.162(6) | 0.6(2) |
| $O_2$ | 1 | 0.15(1) | 0.49(1) | 0.194(4) | $B(O_1)$ |
| $O_3$ | 1 | 0.356(7) | 0.033(4) | 0.477(2) | $B(O_1)$ |

*Continued*


https://doi.org/10.1017/S0885715614000803 Published online by Cambridge University Press

TABLE II. Continued

| | | | | | |
|---|---|---|---|---|---|
| Group (iii) | | | | | |
| $O_4$ | 1 | 0.48(1) | 0.15(1) | 0.171(6) | $B(O_1)$ |
| $Ba_3MgSi_2O_8$ ($x = 3$) | | | | | |
| $Ba_1/Sr_1$ | 1 | 0.333(1) | 0.334(2) | 0.1776(3) | 0.41(5) |
| $Ba_2/Sr_2$ | 1 | 1/3 | 2/3 | 0.506(1) | 0.82(8) |
| $Ba_3/Sr_3$ | 1 | 0 | 0 | 1/2 | $B(Ba_2/Sr_2)$ |
| $Mg_1$ | 1 | 1/3 | 2/3 | 0.010(7) | 0.9(3) |
| $Mg_2$ | 1 | 0 | 0 | 0 | $B(Mg_1)$ |
| Si | 1 | 0.336(7) | 0.006(3) | 0.260(1) | 0.3(2) |
| $O_1$ | 1 | 0.00(2) | 0.18(1) | 0.191(6) | 0.9(3) |
| $O_2$ | 1 | 0.16(1) | 0.49(1) | 0.187(5) | $B(O_1)$ |
| $O_3$ | 1 | 0.349(6) | 0.045(3) | 0.475(3) | $B(O_1)$ |
| $O_4$ | 1 | 0.49(1) | 0.16(1) | 0.154(4) | $B(O_1)$ |

accompanied by a disappearance of mirror planes and of 2/3 of threefold axes. Figure 5 shows Ba-content ($x$ in $Ba_xSr_{3-x}MgSi_2O_8$) dependence of the cell size. To compare unit cells with different $Z$-values, cell parameters were converted to those of the corresponding trigonal cells of $Z = 1$ with the relations that $a_t = b_m = a_T/\sqrt{3}$ and $c_t = c_m \sin\beta/2 = c_T$ [subscript "m" means a monoclinic cell ($Z = 4$) of the group (i), "t" a trigonal cell ($Z = 1$) of group (ii), and "T" a trigonal cell ($Z = 3$) of group (iii)]. It can be seen that unit-cell size monotonically increases with increasing Ba-content ($x$). However, the increase rate for parameter $c$ changes at $x = 0.5$. At this point, the crystal system changes between monoclinic and trigonal. Details of the structural change caused by Ba/Sr ratio are discussed in the 'Discussion' section.

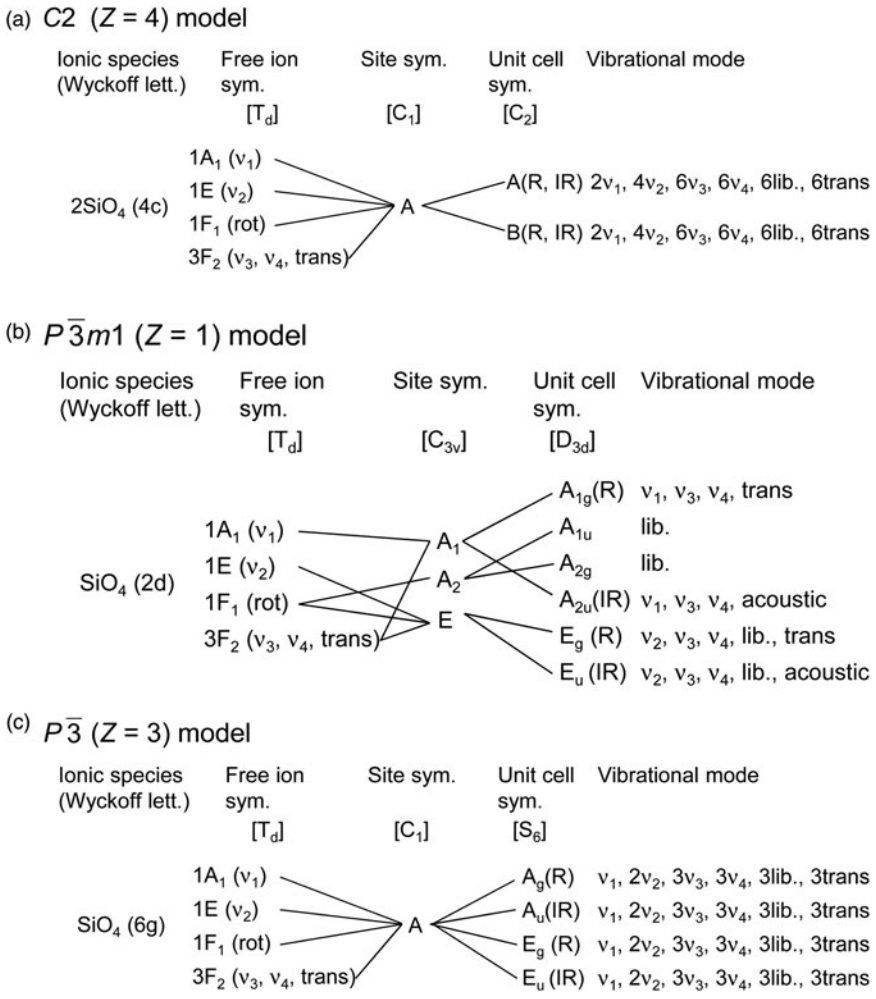



Figure 4. Correlation tables for $SiO_4$ tetrahedra in $Ba_xSr_{3-x}MgSi_2O_8$; (a) $C2$, (b) $P\bar{3}m1$, and (c) $P\bar{3}$. R and IR indicate Raman active and IR active, respectively.


https://doi.org/10.1017/S0885715614000803 Published online by Cambridge University Press

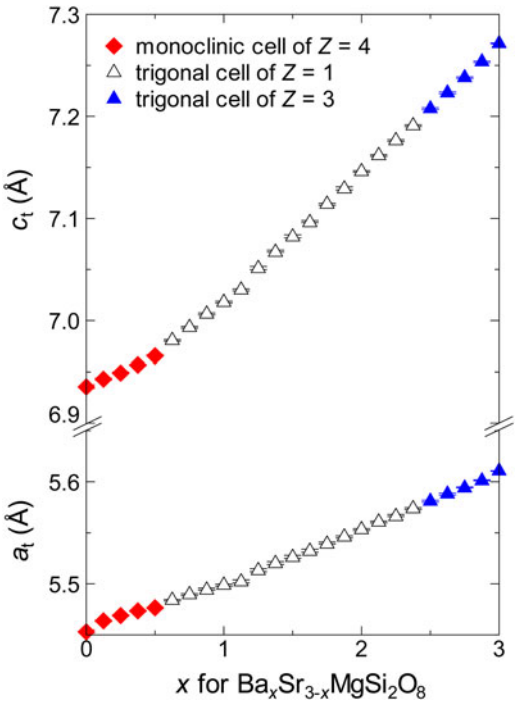



Figure 5. (Color online) Ba/Sr-ratio dependence of $Ba_xSr_{3-x}MgSi_2O_8$ cell size. Unit-cell parameters were converted to $a_t$ and $c_t$ ($Z$=1) with the equations described in Section 3.2. Data-point shape indicates the type of the original cell. Closed diamonds, open and closed triangles correspond to monoclinic cells of $Z = 4$, trigonal cells of $Z = 1$ and of $Z = 3$, respectively.

## IV. Discussion

Figure 6 shows the change in $Ba_xSr_{3-x}MgSi_2O_8$ structure caused by Ba/Sr replacement. As described in the Introduction section, $Ba_xSr_{3-x}MgSi_2O_8$ is composed of layers of corner-sharing $SiO_4$ and $MgO_6$. $Ba^{2+}$ and $Sr^{2+}$ ions are sandwiched in between the layers. Structural refinement (Tables I and II) reveals that $Ba^{2+}$ preferentially occupies the interlayer A-site. The observed structure change can be traced in association with this site selectivity. Firstly, we focus on $BaSr_2MgSi_2O_8$ [$x = 1.000$, Figure 6(b)]. At this composition, Ba:Sr atomic ratio is 1:2, which corresponds with the ratio of A- to B-sites. In this compound, almost all $Ba^{2+}$ ions occupy A-site and $Sr^{2+}$ ions B-site. The Si–$O_2$ dangling bonds protruding from the flat layers are coaxial with threefold rotation axes. They directly face to the neighboring B-site cations and make Si–O–B pillars perpendicular to the layers.

As Ba/Sr ratio decreases from the above situation, A-site $Ba^{2+}$ is gradually replaced by $Sr^{2+}$. Simultaneously, the average size of A-site cations is reduced. The smaller A-site cation is accommodated by narrowing interlayer spaces. However, the narrowing rate is low, as shown in Figure 5, because the interlayer spaces are supported by Si–O–B($Sr^{2+}$) pillars. In the compounds of $x \leq 1$, structural fluctuation is presumably present at A-site, as seen in the sudden increase in the isotropic atomic displacement parameter $B$ for A-site cation (~0.7 for $x > 1$ and ~1.0 for $x \leq 1$; Table II). For $x < 0.5$ [group (i)], $SiO_4$ tetrahedra tilt to adjust space laterally for the smaller A-site cation, which makes the layers corrugated and misalign. As a result, lattice leans slightly and the crystal

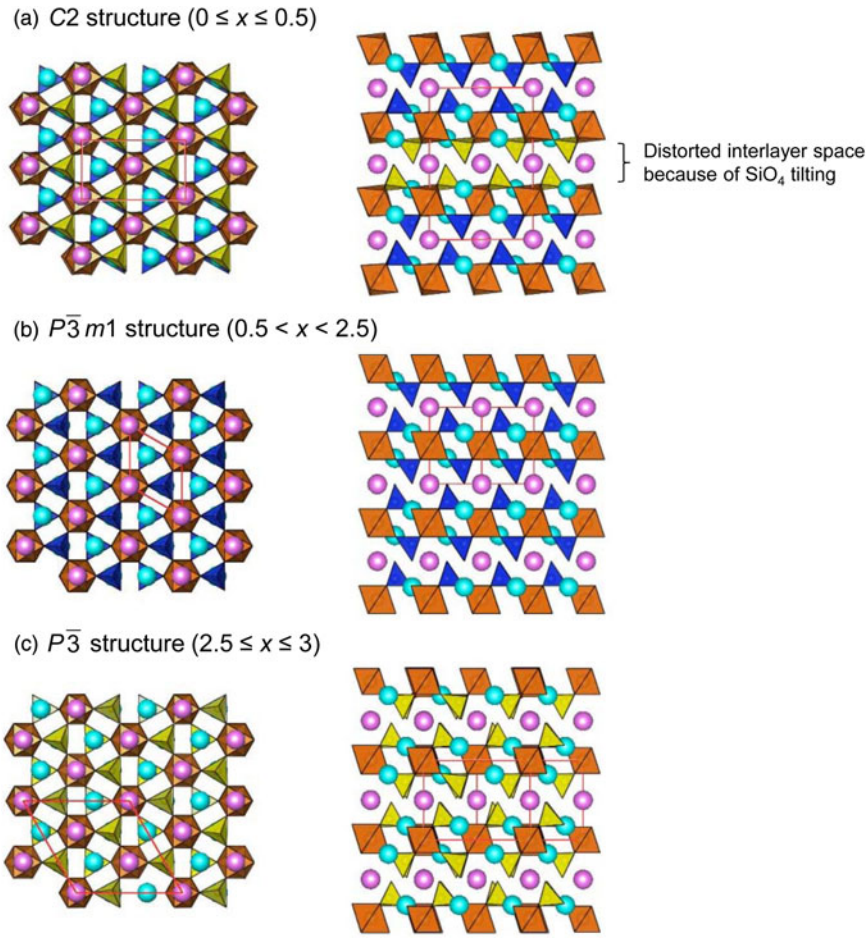



Figure 6. (Color online) Crystal structure of $Ba_xSr_{3-x}MgSi_2O_8$ illustrated with $SiO_4$ tetrahedra and $MgO_6$ octahedra. A- and B-site cations are given by pink and light blue spheres, respectively. Red solid line frames indicate unit cells. Tilted $SiO_4$ tetrahedra are highlighted in yellow color.


https://doi.org/10.1017/S0885715614000803 Published online by Cambridge University Press

structure loses all the threefold rotation axes ($P\bar{3}m1 \rightarrow C2/m$, $\mathbf{a}_m = 2\mathbf{a}_t + \mathbf{b}_t$, $\mathbf{b}_m = \mathbf{b}_t$, $\mathbf{c}_m = 2\mathbf{c}_t$) and mirror planes ($C2/m \rightarrow C2$), leading to a monoclinic unit cell of $C2$. It should be noted that the $SiO_4$ tilting starts every other interlayer space (Figure 6, $SiO_4$ in yellow color). Similar structural aspect has been reported for an isostructural silicate $(Ba_{0.65}Ca_{0.35})_2SiO_4$. Fukuda *et al.* (2007) set the space group $P\bar{3}m1$, and identified that $SiO_4$ tilted every other interlayer. In $(Ba_{0.65}Ca_{0.35})_2SiO_4$, the position of the A-site cation in the distorted interlayer space was not definitely determined. This fact corresponds to the large atomic displacement parameter for A-site in the present case. As for the limiting case of $x = 0$, $R_{wp}$ is still large even for a $C2$ model. Considering the Raman spectra, $Sr_3MgSi_2O_8$ may have a lower-symmetry structure.

On the other hand, for $x > 1$, excess $Ba^{2+}$ ions are forced to be placed at the layer-embedded B-site, which leads to an increase in the average size of B-site cations. Then, interlayer spaces linearly increase, because Si–O–B pillars elongate in response to the size increase. The $P\bar{3}m1$ ($Z = 1$) structure can accommodate the B-site cation enlargement until $x = 2.375$. However, this structure has inherent instability as is clear from the presence of an impurity phase (Figure 3). It is considered that the instability originates in two geometric factors: (i) size exclusion by pockets on the layer, and (ii) steric hindrance from dangling Si–O bonds. Since the former factor has been pointed out in my previous report (Yonesaki *et al.*, 2009), we treat the latter in this study. Focusing on the Si–O dangling bonds, their bond lengths (between 1.57 and 1.59 Å) are shorter than that expected from Shannon's ionic radii (1.66 Å) (Shannon, 1976). For $Ba_{2.500}Sr_{0.500}MgSi_2O_8$ ($x = 2.500$), the Si–O distance becomes much shorter (1.53 Å). This compression may be because of the capping by the adjacent B-site cation, considering the linear relationship between $c_t$ and $x$ (Figure 5). Above this limit, Si–O dangling bonds tilt to relax the steric hindrance [group (iii), Figure 6(c)]. Consequently, $Ba_xSr_{3-x}MgSi_2O_8$ loses 2/3 of threefold axes and all the mirror planes, leading to the formation of $P\bar{3}$ structure with $Z = 3$.

## V. Conclusion

$Ba_xSr_{3-x}MgSi_2O_8$ structure change caused by Ba/Sr replacement has been traced using Raman spectroscopy and X-ray powder diffraction. The solid solution series has layered glaserite-type structure in which larger $Ba^{2+}$ ions preferentially occupy interlayer A-site. As for $BaSr_2MgSi_2O_8$, since the ratio of the number of A-site to that of B-site is 1:2, $Ba^{2+}$ and $Sr^{2+}$ occupy A- and B-sites, respectively. In the case of $x < 1$, the average size of A-site cations is smaller than $Ba^{2+}$, because $Sr^{2+}$ ions replace $Ba^{2+}$ at A-site. In an extreme case of $x \leq 0.5$, $SiO_4$ tetrahedra tilt to fit the smaller A-site cations, and the layers made of corner-sharing $SiO_4$ tetrahedra and $MgO_6$ octahedra become corrugated. As for the case of $x \geq 1$, that is, Ba:Sr ratio exceeds that of A-site:B-site, the average size of B-site cations becomes larger than $Sr^{2+}$ because excess $Ba^{2+}$ ions are forced to be placed at B-site. However, the size mismatch between the enlarged B-site cations and B-site spaces results in the formation of $BaMgSiO_4$ and in $SiO_4$ tilting.


## ACKNOWLEDGEMENT

The author, Y. Yonezaki is indebted to the financial support for the present research by Nippon Sheet Glass Foundation for Materials Science and Engineering.


## SUPPLEMENTARY MATERIALS AND METHODS

The supplementary material refered to in this paper can be found online at journals.cambridge.org/pdj.


Aitasalo, T., Hietikko, A., Hölsä, J., Lastusaari, M., Niittykoski, J., and Piispanen, T. (**2007**). "Crystal structure of the $Ba_3MgSi_2O_8:Mn^{2+}$, $Eu^{2+}$ phosphor for white light emitting diodes," Z. Kristallogr. Suppl. **26**, 461–466.

Barry, T. L. (**1968**). "Equilibria and $Eu^{2+}$ luminescence of subsolidus phases bounded by $Ba_3MgSi_2O_8$, $Sr_3MgSi_2O_8$, and $Ca_3MgSi_2O_8$," J. Electrochem. Soc. **115**, 733–738.

Fu, C., Hu, Y., Wang, Y., Wu, H., and Wang, X. (**2010**). "Luminescent properties of the $Sr_{2.97-x}Ba_xMgSi_2O_8:Eu^{2+}{}_{0.01}$, $Dy^{3+}{}_{0.02}$ with different Sr/Ba ratio," J. Alloys Compd. **502**, 423–428.

Fukuda, K., Ito, M., and Iwata, T. (**2007**). "Crystal structure and structural disorder of $(Ba_{0.65}Ca_{0.35})_2SiO_4$," J. Solid State Chem. **180**, 2305–2309.

Gromov, V. V. and Morton, J. R. (**1966**). "Paramagnetic centers in irradiated potassium sulfate," Can. J. Chem. **44**, 527–528.

Hayakawa, T. and Ohta, M. (**1999**). "Role of dopant on the formation of $SO_3^-$ radical induced by X-ray irradiation in $K_3Na(SO_4)_2$," J. Lumin. **81**, 313–319.

Im, W. B., Kim, Y. I., Yoo, H. S., and Jeon, D. Y. (**2009**). "Luminescent and structural properties of $(Sr_{1-x},Ba_x)_3MgSi_2O_8:Eu^{2+}$: effects of Ba content on the $Eu^{2+}$ site preference for thermal stability," Inorg. Chem. **48**, 557–564.

Iwata, T., Horie, T., and Fukuda, K. (**2009**). "Reinvestigation of crystal structure and structural disorder of $Ba_3MgSi_2O_8$," Powder Diffr. **24**, 180–184.

Izumi, F. and Momma, K. (**2007**). "Three-dimensional visualization in powder diffraction," Solid State Phenom. **130**, 15–20.

Jung, H. K. and Seo, K. S. (**2006**). "Luminescent properties of $Eu^{2+}$-activated $(Ba, Sr)_3MgSi_2O_8$ phosphor under VUV irradiation," Opt. Mater. **28**, 602–605.

Kaczmarski, M. and Mróz, B. (**1998**). "Raman study of the ferroelastic phase transition in $K_3Na(SeO_4)_2$," Phys. Rev. B **57**, 13589–13598.

Kaczmarski, M., Mróz, B., Kiefte, H., Clouter, M. J., and Rich, N. H. (**1994**). "Raman studies of lattice vibrations in ferroelastic $K_3Na(SeO_4)_2$," Ferroelectrics **152**, 331–335.

Kim, J. S., Lim, K. T., Jeong, Y. S., Jeon, P. E., Choi, J. C., and Park, H. L. (**2005**). "Full-color $Ba_3MgSi_2O_8:Eu^{2+}$, $Mn^{2+}$ phosphors for white-light-emitting diodes," Solid State Commun. **135**, 21–24.

Krajewski, T., Piskunowicz, P., and Mróz, B. (**1993**). "Structural phase transitions in $K_3Na(SeO_4)_2$ crystals," Phys. Status Solidi **135**, 557–564.

Lin, Y., Tang, Z., Zhang, Z., and Nan, C. W. (**2003**). "Luminescence of $Eu^{2+}$ and $Dy^{3+}$ activated $R_3MgSi_2O_8$-based (R = Ca, Sr, Ba) phosphors," J. Alloys Compd. **348**, 76–79.

Momma, K. and Izumi, F. (**2011**). "VESTA 3 for three-dimensional visualization of crystal, volumetric and morphology data," J. Appl. Crystallogr. **44**, 1272–1276.

Mróz, B., Kiefte, H., Clouter, M. J., and Tuszyński, J. A. (**1992**). "Ferroelastic phase transition in $K_3Na(SeO_4)_2$: Brillouin-scattering studies and theoretical modeling," Phys. Rev. B **46**, 8717–8724.

Ohta, M., Hayakawa, T., and Furukawa, H. (**2000**). "Dose quality determined using ESR imaging," Radiat. Meas. **32**, 147–151.

Okamoto, S., Nanba, Y., Honma, T., and Yamamoto, (**2008**). "Ba-substitution effect on luminescent properties and thermal degradation of $Sr_3MgSi_2O_8:Eu^{2+}$ blue phosphor under vacuum–UV–light excitation," J. Electrochem. Solid-State Lett. **11**, J47–J49.

Park, C. H., Hong, S. T., and Keszler, D. A. (**2009**). "Superstructure of a phosphor material $Ba_3MgSi_2O_8$ determined by neutron diffraction data," J. Solid State Chem. **182**, 496–501.

Park, C. H., Kim, T. H., Yonesaki, Y., and Kumada, N. (**2011**). "A re-investigation of the crystal structure and luminescence of $BaCa_2MgSi_2O_8:Eu^{2+}$," J. Solid State Chem. **184**, 1566–1570.





https://doi.org/10.1017/S0885715614000803 Published online by Cambridge University Press

Remy, C., Reynard, B., and Madon, M. (**1997**). "Raman spectroscopic investigations of dicalcium silicate: polymorphs and high-temperature phase transformations," J. Am. Ceram. Soc. **80**, 413–423.

Shannon, R. D. (**1976**). "Revised effective ionic radii and systematic studies of interatomic distances in halides and chalcogenides," Acta Crystallogr. A **32**, 751–767.

Werner, P. E., Eriksson, L., and Westdahl, M. (**1985**). "TREOR, a semi-exhaustive trial–and–error powder indexing program for all symmetries," J. Appl. Crystallogr. **18**, 367–370.

Yonesaki, Y. (**2013**). "Structural consideration on the emission properties of $Eu^{2+}$-doped $Ba(Sr, Ca)_2MgSi_2O_8$," J. Solid State Chem. **201**, 324–329.

Yonesaki, Y., Takei, T. Kumada, N. and Kinomura, N. (**2008**). "Crystal structure of $BaCa_2MgSi_2O_8$ and the photoluminescent properties activated by $Eu^{2+}$," J. Lumin. **128**, 1507–1514.

Yonesaki, Y., Takei, T., Kumada, N., and Kinomura, N. (**2009**). "Crystal structure of $Eu^{2+}$–doped $M_3MgSi_2O_8$ (*M*: Ba, Sr, Ca) compounds and their emission properties," J. Solid State Chem. **182**, 547–554.



https://doi.org/10.1017/S0885715614000803 Published online by Cambridge University Press